Available online at www.sciencedirect.com
SCIENCE DIRECT
International Journal of Heat and Mass Transfer 49 (2006) 695–706
International Journal of HEAT and MASS TRANSFER
www.elsevier.com/locate/ijhmt

Averaging approach for microchannel heat sinks subject to the uniform wall temperature condition

Dong-Kwon Kim, Sung Jin Kim *

Department of Mechanical Engineering, Korea Advanced Institute of Science and Technology, Daejeon 305-701, Republic of Korea

Received 23 March 2005; received in revised form 17 August 2005
Available online 19 October 2005

Abstract

The present paper is devoted to modeling methods for thermal analysis of microchannel heat sinks. The averaging approach presented in earlier works for the case of constant surface heat flux is extended to the problems subject to the uniform wall temperature condition. The solutions for velocity and temperature distributions are obtained by solving one-dimensional averaged governing equations without resorting to a two-dimensional direct numerical simulation. General solutions for both high-aspect-ratio and low-aspect-ratio microchannel heat sinks are presented. Asymptotic solutions in high-aspect-ratio and low-aspect-ratio limits are also given in explicit form. The solutions presented in the paper are validated by comparing them with the results of direct numerical simulation. The friction factors, Nusselt numbers and thermal resistances for microchannel heat sinks with a uniform base temperature are obtained from the presented solutions. The effects of the aspect ratio and the porosity on the friction factor and the Nusselt number are presented. Finally, characteristics of the thermal resistance of the microchannel heat sink are discussed.

1. Introduction

Recent advances in semiconductor technology have led to the significant increase in power densities encountered in microelectronic equipment [1,2]. Therefore, effective cooling technology is essential for reliable operation of electronic components [3,4]. Microchannel heat sinks have received much attention due to their high potential for cooling electronic devices. The concept of the microchannel heat sink was first introduced by Tuckerman and Pease [5] and is based on the fact that the heat transfer coefficient is inversely proportional to the hydraulic diameter of the channel. Since the emergence of this technology, a body of research has been reported, as summarized in the extensive reviews by Phillips [6] and by Goodling and Knight [7].

Many previous investigations have been concentrated on compact modeling methods for the microchannel heat sink. It is because direct numerical simulation requires tedious effort and large computation time. The simplest modeling method is to use a fin model [8,9]. The fin model is commonly used due to its simplicity [10], but it was recently confirmed that the fin model may produce errors in predicting the thermal resistance when the aspect ratio of the microchannel is high [11,12]. As an alternative, Koh and Colony [13] suggested a model based on an averaging approach. In this model, the microchannel heat sink is modeled as a fluid-saturated porous medium, which is frequently termed the porous-medium approach. Mathematically, this is equivalent to averaging the velocity and temperature distributions in the direction perpendicular to the flow direction. This approach was applied to the microchannel heat sink by Tien and Kuo [14] and later extended by Kim and his coworkers [15–17]. Analytic solutions suggested by Kim and his coworkers are shown to be in close agreement with numerical solutions and their model predicts the thermal resistance accurately.

Even though the model based on the averaging approach for predicting the thermal resistance has been suggested, it has focused only on the uniform wall heat flux condition. Hence, it could not be used to delineate fluid-flow and heat-transfer characteristics of the microchannel

* Corresponding author. Tel.: +82 42 869 3043; fax: +82 42 869 3210.
E-mail address: sungjinkim@kaist.ac.kr (S.J. Kim).

0017-9310/$ - see front matter © 2005 Elsevier Ltd. All rights reserved.
doi:10.1016/j.ijheatmasstransfer.2005.08.012

Nomenclature

a	wetted area per volume
c	heat capacity of fluid
Da	Darcy number
D_h	hydraulic diameter of the channel ($2w_cH/(w_c+H)$)
f	friction factor
h	interstitial heat transfer coefficient based on one-dimensional bulk mean temperature
h_l	interstitial heat transfer coefficient
H	channel height
k	thermal conductivity
K	permeability
L	length of heat sink
Nu	Nusselt number
p	pressure
P	dimensionless pressure
Pe	Peclet number
q	heat transfer rate
q''	heat flux (q/WL)
$\dot{Q}$	flow rate
Re	Reynolds number
R_θ	total thermal resistance
T	temperature
u	velocity
U	dimensionless velocity
w_c	channel width
w_w	fin thickness
W	width of heat sink
x,y,z	Cartesian coordinate system
X,Y,Z	dimensionless Cartesian coordinate system ($Y=y/H$, $Z=z/(w_c+w_w)$)
$\langle\rangle^f$	averaged value over the fluid region
$\langle\rangle^s$	averaged value over the solid region
$\langle T\rangle^{b,f}$	one-dimensional bulk mean temperature for the fluid phase

Greek symbols

α_s	aspect ratio of the microchannel (H/w_c)
ε	porosity ($w_c/(w_c+w_w)$)
λ	dimensionless eigenvalue
μ	viscosity
θ	dimensionless temperature
ρ	density

Subscripts

bm	bulk mean
e	effective
f	fluid
high	for high-aspect-ratio microchannel heat sinks ($\alpha_s>1$)
H5	exponential axial wall heat flux condition
in	inlet
low	for low-aspect-ratio microchannel heat sinks ($\alpha_s<1$)
m	mean
out	outlet
s	solid
w	wall
y	averaging direction: y
z	averaging direction: z

heat sink subject to the uniform surface temperature condition. However, the base wall of the microchannel heat sink becomes nearly isothermal when it is thick enough to eliminate hot spots or it is attached to a heat spreader such as a vapor chamber and a micro heat pipe [18]. Therefore, it is highly desirable to develop an appropriate mathematical model for analyzing heat transfer from a microchannel heat sink subject to the constant wall temperature condition.

The present study is devoted to overcoming the limitation stated above by extending the previous works [15–17] to the problems for the uniform wall temperature condition. The present study deals with a modeling method based on an averaging approach for thermal analysis of microchannel heat sinks subject to the uniform wall temperature condition. General solutions for both high-aspect-ratio and low-aspect-ratio microchannel heat sinks are presented. Asymptotic solutions in high-aspect-ratio and low-aspect-ratio limits are given in explicit form by using the scale analysis. In order to validate the proposed solutions, velocity and temperature distributions obtained from the general solutions and the asymptotic solutions are compared with results from two-dimensional direct numerical simulation. The friction factors, Nusselt numbers and thermal resistances for microchannel heat sinks with a uniform base temperature are obtained from the presented solutions. The effects of the aspect ratio and the porosity on the friction factor and the Nusselt number are investigated. Finally, characteristics of the thermal resistance of the microchannel heat sink are discussed.

2. Mathematical formulation by using averaging approach

2.1. Problem description

The problem under consideration in the present paper concerns forced convection through a microchannel heat sink. Schematic diagrams of the microchannel heat sink are shown in Fig. 1. The direction of fluid flow is parallel to x. The top surface is insulated and the bottom surface is isothermal. A coolant passes through microchannels and it takes heat away from the heat dissipating electronic

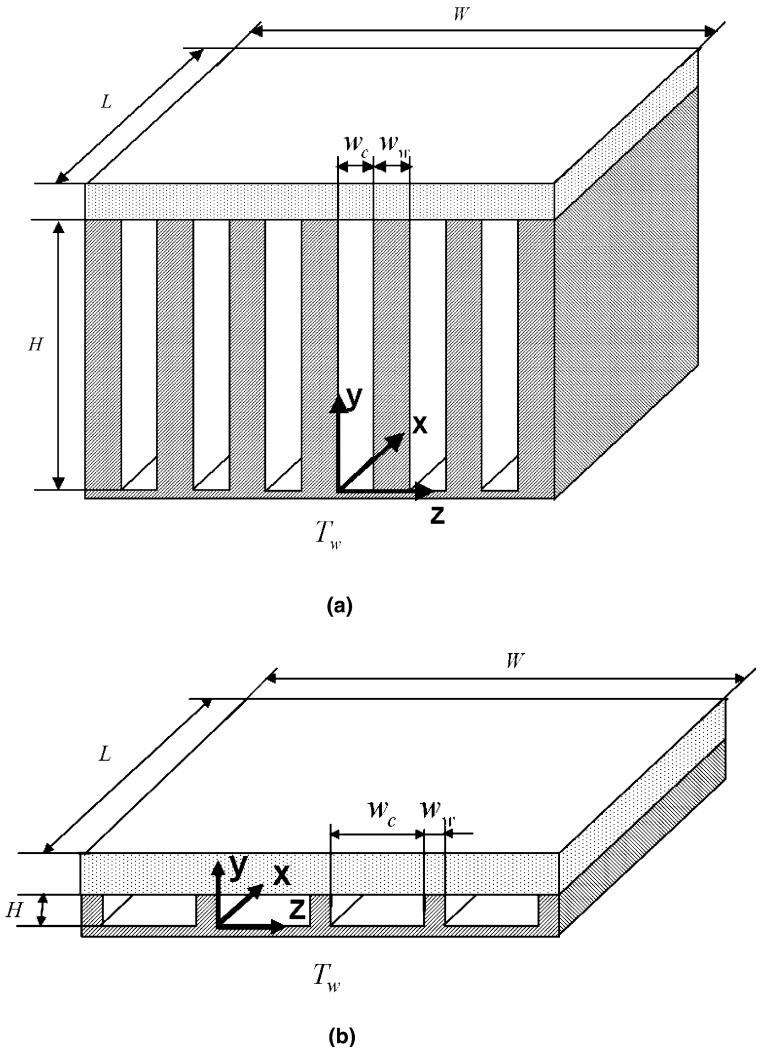

Fig. 1. Schematic diagrams of microchannel heat sinks: (a) high-aspect-ratio microchannel heat sink ($\alpha_s > 1$) and (b) low-aspect-ratio microchannel heat sink ($\alpha_s < 1$).

component attached below. In analyzing the problem, for simplicity, the flow is assumed to be laminar, incompressible, and both hydrodynamically and thermally fully-developed. All the thermophysical properties are assumed to be constant. In addition, the pumping power, i.e., the power required to drive the fluid through the microchannels, is assumed to be constant.

2.2. General solutions

2.2.1. General solutions for high-aspect-ratio microchannel heat sinks

The momentum and energy equations are given as follows:

$$\frac{\partial p}{\partial x} = \mu\left(\frac{\partial^2 u}{\partial y^2} + \frac{\partial^2 u}{\partial z^2}\right) \tag{1}$$

$$\rho c \frac{\partial (uT)}{\partial x} = k\left(\frac{\partial^2 T}{\partial y^2} + \frac{\partial^2 T}{\partial z^2}\right) \tag{2}$$

In the averaging approach, averaged velocity and temperature are used. The averaged quantities over the fluid and solid phases are defined, respectively, as follows:

$$\langle \phi \rangle_z^{\mathrm{f}} = \frac{1}{w_{\mathrm{c}}} \int_0^{w_{\mathrm{c}}} \phi \, \mathrm{d}z, \quad \langle \phi \rangle_z^{\mathrm{s}} = \frac{1}{w_{\mathrm{w}}} \int_{w_{\mathrm{c}}}^{w_{\mathrm{w}}+w_{\mathrm{c}}} \phi \, \mathrm{d}z \tag{3}$$

The governing equations for averaged velocity and temperature are established by averaging Eqs. (1) and (2) in the z direction. Integrating Eq. (1) over the fluid region yields

$$\frac{\partial \langle p \rangle_z^{\mathrm{f}}}{\partial x} = \mu_{\mathrm{f}} \frac{\partial^2 \langle u \rangle_z^{\mathrm{f}}}{\partial y^2} - \frac{\mu_{\mathrm{f}}}{K_{\mathrm{high}}} \varepsilon \langle u \rangle_z^{\mathrm{f}} \tag{4}$$

Similarly, averaging Eq. (2) over the fluid region produces

$$\varepsilon \rho_{\mathrm{f}} c_{\mathrm{f}} \frac{\partial \langle uT \rangle_z^{\mathrm{f}}}{\partial x} = \frac{\partial}{\partial y}\left(k_{\mathrm{fe,high}} \frac{\partial \langle T \rangle_z^{\mathrm{f}}}{\partial y}\right) + h_{\mathrm{l,high}} a_{\mathrm{high}} (\langle T \rangle_z^{\mathrm{s}} - \langle T \rangle_z^{\mathrm{f}}) \tag{5}$$

and the energy equation for the solid region becomes

$$\frac{\partial}{\partial y}\left(k_{\mathrm{se,high}}\frac{\partial\langle T\rangle_z^{\mathrm{s}}}{\partial y}\right)=h_{\mathrm{l,high}}a_{\mathrm{high}}(\langle T\rangle_z^{\mathrm{s}}-\langle T\rangle_z^{\mathrm{f}}) \tag{6}$$

where ε, a, k_{fe}, k_{se}, K, and h_{l} are porosity, wetted area per volume, effective conductivity of the fluid, effective conductivity of the solid, permeability, and interstitial heat transfer coefficient, respectively. The subscript high is used to distinguish this case from the case of *low*-aspect-ratio microchannel heat sinks.

$$\varepsilon=\frac{w_{\mathrm{c}}}{w_{\mathrm{w}}+w_{\mathrm{c}}},\quad a_{\mathrm{high}}=\frac{2}{w_{\mathrm{w}}+w_{\mathrm{c}}},$$
$$k_{\mathrm{se,high}}=(1-\varepsilon)k_{\mathrm{s}},\quad k_{\mathrm{fe,high}}=\varepsilon k_{\mathrm{f}} \tag{7}$$

$$K_{\mathrm{high}}=-\varepsilon w_{\mathrm{c}}\langle u\rangle_z^{\mathrm{f}}\left(\left.\frac{\partial u}{\partial z}\right|_{z=w_{\mathrm{c}}}-\left.\frac{\partial u}{\partial z}\right|_{z=0}\right)^{-1} \tag{8}$$

$$h_{\mathrm{l,high}}=\frac{k_{\mathrm{f}}}{2}\left(\left.\frac{\partial T}{\partial z}\right|_{z=w_{\mathrm{c}}}-\left.\frac{\partial T}{\partial z}\right|_{z=0}\right)\cdot(\langle T\rangle_z^{\mathrm{s}}-\langle T\rangle_z^{\mathrm{f}})^{-1} \tag{9}$$

In order to treat the averaged quantities for a product of temperature and velocity $\langle uT\rangle_z^{\mathrm{f}}$ involved in Eq. (5), it is useful to define the one-dimensional bulk mean temperature for the fluid phase as

$$\langle T\rangle_z^{\mathrm{b,f}}=\frac{\int_0^{w_{\mathrm{c}}}Tu\,\mathrm{d}z}{\int_0^{w_{\mathrm{c}}}u\,\mathrm{d}z} \tag{10}$$

By using the one-dimensional bulk mean temperature, Eqs. (5) and (6) can be rewritten as follows:

$$\varepsilon\rho_{\mathrm{f}}c_{\mathrm{f}}\langle u\rangle_z^{\mathrm{f}}\frac{\partial\langle T\rangle_z^{\mathrm{b,f}}}{\partial x}=\frac{\partial}{\partial y}\left(k_{\mathrm{fe,high}}\frac{\partial\langle T\rangle_z^{\mathrm{b,f}}}{\partial y}\right)+h_{\mathrm{high}}a_{\mathrm{high}}(\langle T\rangle_z^{\mathrm{s}}-\langle T\rangle_z^{\mathrm{b,f}}) \tag{11}$$

$$\frac{\partial}{\partial y}\left(k_{\mathrm{se,high}}\frac{\partial\langle T\rangle_z^{\mathrm{s}}}{\partial y}\right)=h_{\mathrm{high}}a_{\mathrm{high}}(\langle T\rangle_z^{\mathrm{s}}-\langle T\rangle_z^{\mathrm{b,f}}) \tag{12}$$

where h is the interstitial heat transfer coefficient based on one-dimensional bulk mean temperature.

$$h_{\mathrm{high}}=\frac{k_{\mathrm{f}}}{2}\left(\left.\frac{\partial T}{\partial z}\right|_{z=w_{\mathrm{c}}}-\left.\frac{\partial T}{\partial z}\right|_{z=0}\right)\cdot(\langle T\rangle_z^{\mathrm{s}}-\langle T\rangle_z^{\mathrm{b,f}})^{-1} \tag{13}$$

When the flow is thermally fully-developed, it follows that [19]

$$\frac{\partial}{\partial x}\left(\frac{T_{\mathrm{w}}-\langle T\rangle_z^{\mathrm{b,f}}}{T_{\mathrm{w}}-T_{\mathrm{bm}}}\right)=\frac{\partial}{\partial x}\left(\frac{T_{\mathrm{w}}-\langle T\rangle_z^{\mathrm{s}}}{T_{\mathrm{w}}-T_{\mathrm{bm}}}\right)=0 \tag{14}$$

Eq. (14) implies that the relative shape of the temperature profile does not change with x. This equation can be simplified for the conditions of constant surface heat flux and constant surface temperature. For the case of constant surface heat flux, it follows from Eq. (14) that

$$\frac{\partial\langle T\rangle_z^{\mathrm{b,f}}}{\partial x}=\frac{\partial\langle T\rangle_z^{\mathrm{s}}}{\partial x}=\frac{\mathrm{d}T_{\mathrm{bm}}}{\mathrm{d}x} \tag{15}$$

For the case of constant surface temperature, it also follows from Eq. (14) that

$$\frac{\frac{\partial}{\partial x}\langle T\rangle_z^{\mathrm{b,f}}}{T_{\mathrm{w}}-\langle T\rangle_z^{\mathrm{b,f}}}=\frac{\frac{\partial}{\partial x}\langle T\rangle_z^{\mathrm{s}}}{T_{\mathrm{w}}-\langle T\rangle_z^{\mathrm{s}}}=\frac{\frac{\mathrm{d}T_{\mathrm{bm}}}{\mathrm{d}x}}{T_{\mathrm{w}}-T_{\mathrm{bm}}}=\lambda' \tag{16}$$

where λ' is the eigenvalue. Eq. (16) means the temperatures increase exponentially with distance along the streamwise direction. For instance, in the case of the solid temperature

$$T_{\mathrm{w}}-\langle T\rangle_z^{\mathrm{s}}=(T_{\mathrm{w}}-\langle T\rangle_{z,\mathrm{in}}^{\mathrm{s}})\exp(-\lambda' x) \tag{17}$$

For later use we define a dimensionless eigenvalue λ as

$$\lambda=2w_{\mathrm{c}}Pe\lambda'$$

where the Peclet number is

$$Pe=\frac{\rho_{\mathrm{f}}c_{\mathrm{f}}u_{\mathrm{m}}(2w_{\mathrm{c}})}{k_{\mathrm{f}}} \tag{18}$$

Finally, from Eqs. (4), (11), (12) and (16), the governing equations for dimensionless velocity and temperature distributions are given as follows:

$$P_{\mathrm{high}}=Da_{\mathrm{high}}\frac{\mathrm{d}^2U_z^{\mathrm{f}}}{\mathrm{d}Y^2}-U_z^{\mathrm{f}}-\varepsilon\rho_{\mathrm{f}}c_{\mathrm{f}}u_{\mathrm{m}}U_z^{\mathrm{f}}\frac{\lambda}{2w_{\mathrm{c}}Pe}\theta_z^{\mathrm{b,f}} \tag{19}$$

$$=\frac{1}{H^2}\frac{\partial}{\partial Y}\left(k_{\mathrm{fe,high}}\frac{\partial\theta_z^{\mathrm{b,f}}}{\partial Y}\right)+h_{\mathrm{high}}a_{\mathrm{high}}(\theta_z^{\mathrm{s}}-\theta_z^{\mathrm{b,f}}) \tag{20}$$

$$\frac{1}{H^2}\frac{\partial}{\partial Y}\left(k_{\mathrm{se,high}}\frac{\partial\theta_z^{\mathrm{s}}}{\partial Y}\right)=h_{\mathrm{high}}a_{\mathrm{high}}(\theta_z^{\mathrm{s}}-\theta_z^{\mathrm{b,f}}) \tag{21}$$

where

$$P_{\mathrm{high}}=\frac{K_{\mathrm{high}}}{\varepsilon\mu_{\mathrm{f}}u_{\mathrm{m}}}\frac{\mathrm{d}\langle p\rangle_z^{\mathrm{f}}}{\mathrm{d}x},\quad U_z^{\mathrm{f}}=\frac{\langle u\rangle_z^{\mathrm{f}}}{u_{\mathrm{m}}},$$
$$\theta_z^{\mathrm{b,f}}=\frac{\langle T\rangle_z^{\mathrm{b,f}}-T_{\mathrm{w}}}{T_{\mathrm{bm}}-T_{\mathrm{w}}},\quad \theta_z^{\mathrm{s}}=\frac{\langle T\rangle_z^{\mathrm{s}}-T_{\mathrm{w}}}{T_{\mathrm{bm}}-T_{\mathrm{w}}} \tag{22}$$
$$Da_{\mathrm{high}}=\frac{K_{\mathrm{high}}}{\varepsilon H^2},\quad T_{\mathrm{bm}}=\int_0^H\langle T\rangle_z^{\mathrm{b,f}}\,\mathrm{d}y,$$
$$\int_0^1U_z^{\mathrm{f}}\,\mathrm{d}Y=1,\quad \int_0^1\theta_z^{\mathrm{b,f}}\,\mathrm{d}Y=1 \tag{23}$$

To solve the governing equations, Eqs. (19)–(21), the permeability K and the interstitial heat transfer coefficient h should be determined in advance. The permeability is related to the viscous shear stress caused by the fins. The interstitial heat transfer coefficient is related to the convective heat transfer from the fins. As pointed out in Slattery [20], we lose some information with any averaging approach: in the present case, the dependence of the velocity and temperature distributions for the fluid phase in the averaging direction. In the averaging approach, we typically replace the lost information with empirical data for K and h. For the present configuration, however, these parameters can be determined analytically through an approximation. For this, it is assumed that the characteristics of pressure drop and heat transfer from the fins are similar to those of the Poiseuille flow between two infinite

parallel plates. The velocity distribution for the Poiseuille flow in this configuration can be easily determined to be

$$u = 6\langle u\rangle_z^{\mathrm{f}} \cdot \frac{z}{w_{\mathrm{c}}}\left(1-\frac{z}{w_{\mathrm{c}}}\right) \tag{24}$$

Using Eq. (24), the permeability is obtained from its definitions, Eq. (8), as

$$K_{\mathrm{high}} = \frac{\varepsilon w_{\mathrm{c}}^2}{12} \tag{25}$$

In order to obtain the interstitial heat transfer coefficient, we use the Nusselt number for the Poiseuille flow between two infinite parallel plates subject to the exponential wall heat flux in the streamwise direction, because the heat flux from the fins exponentially decreases along the streamwise direction. The Nusselt number is available in Ref. [21] and given as the following equation:

$$Nu_{\mathrm{H5}} = \frac{h_{\mathrm{high}} \cdot 2w_{\mathrm{c}}}{k_{\mathrm{f}}} = \frac{3}{8}\left[\sum_{n=1}^{\infty} \frac{-C_n Y_n(1)\beta_n^2}{(32/3)\beta_n^2 - \lambda}\right]^{-1} \tag{26}$$

From Eq. (26), a correlation for the interstitial heat transfer coefficient is obtained as

$$h_{\mathrm{high}} = \frac{k_{\mathrm{f}}}{2w_{\mathrm{c}}} \cdot (8.2426 - 0.0230\lambda) \tag{27}$$

Once the permeability and the interstitial heat transfer coefficient are determined, velocity and temperature distributions can be obtained by solving Eqs. (19)–(21). The general solution for the dimensionless velocity is given as

$$U_z^{\mathrm{f}} = -P_{\mathrm{high}}\left(1 - \frac{\cosh\left(\frac{1}{\sqrt{Da_{\mathrm{high}}}}\left(Y-\frac{1}{2}\right)\right)}{\cosh\left(\frac{1}{2\sqrt{Da_{\mathrm{high}}}}\right)}\right) \tag{28}$$

where

$$P_{\mathrm{high}} = -\left(1 - 2\sqrt{Da_{\mathrm{high}}}\tanh\left(\frac{1}{2\sqrt{Da_{\mathrm{high}}}}\right)\right)^{-1} \tag{29}$$

The dimensionless temperatures $\theta_z^{\mathrm{b,f}}$, θ_z^{s} and the dimensionless eigenvalue λ can be obtained by solving Eqs. (20), (21) and (27) iteratively. For instance, the method of successive approximation introduced in Ref. [22] can be used. This technique consists of guessing a particular polynominal for $\theta_z^{\mathrm{b,f}}$, substituting this guess into the left-hand side of Eq. (20), and finally solving Eqs. (20), (21) and (27) to obtain a better guess for $\theta_z^{\mathrm{b,f}}$. The procedure can be repeated until the change in the λ value from one approximation to the next is below a pre-determined percentage. It is worth mentioning that the last relation of Eq. (23) needs to be employed in this procedure. Without this relation it is impossible to solve Eqs. (20), (21) and (27) and to obtain the better guess for $\theta_z^{\mathrm{b,f}}$.

2.2.2. General solutions for low-aspect-ratio microchannel heat sinks

Temperature and velocity distributions for low-aspect-ratio microchannel heat sinks can be obtained by similar method to that for high-aspect-ratio microchannel heat sinks. The only difference in the averaging method is the direction of averaging. While the averaging is performed in the z-direction for high-aspect-ratio microchannels, it is in the y-direction for low-aspect-ratio microchannels. For the present case, an averaged quantity is defined as

$$\langle\phi\rangle_y = \frac{1}{H}\int_0^H \phi\,\mathrm{d}y \tag{30}$$

In addition, it is useful to define the one-dimensional bulk mean temperature for the fluid phase as

$$\langle T\rangle_y^{\mathrm{b,f}} = \frac{\int_0^H Tu\,\mathrm{d}y}{\int_0^H u\,\mathrm{d}y} \tag{31}$$

The governing equations for averaged velocity and temperature are established by averaging Eqs. (1) and (2) in the y-direction. As a result, the governing equations for dimensionless velocity and temperature distributions are given as follows:

For the fluid phase,

$$P_{\mathrm{low}} = Da_{\mathrm{low}}\frac{\mathrm{d}^2U_y^{\mathrm{f}}}{\mathrm{d}Z^2} - U_y^{\mathrm{f}} \tag{32}$$

$$-\rho_{\mathrm{f}}c_{\mathrm{f}}u_{\mathrm{m}}U_y^{\mathrm{f}}\frac{\lambda}{2w_{\mathrm{c}}Pe}\theta_y^{\mathrm{b,f}} = \frac{1}{(w_{\mathrm{c}}+w_{\mathrm{w}})^2}\frac{\partial}{\partial Z}\left(k_{\mathrm{fe,low}}\frac{\partial\theta_y^{\mathrm{b,f}}}{\partial Z}\right) - h_{\mathrm{low}}a_{\mathrm{low}}\theta_y^{\mathrm{b,f}} \tag{33}$$

For the solid phase,

$$\theta_y^{\mathrm{s}} = 0 \tag{34}$$

where

$$a_{\mathrm{low}} = \frac{1}{H}, \quad k_{\mathrm{fe,low}} = k_{\mathrm{f}} \tag{35}$$

$$P_{\mathrm{low}} = \frac{K_{\mathrm{low}}}{\varepsilon\mu_{\mathrm{f}}u_{\mathrm{m}}}\frac{\mathrm{d}\langle p\rangle_y^{\mathrm{f}}}{\mathrm{d}x}, \quad U_y^{\mathrm{f}} = \frac{\langle u\rangle_y^{\mathrm{f}}}{u_{\mathrm{m}}},$$
$$\theta_y^{\mathrm{b,f}} = \frac{\langle T\rangle_y^{\mathrm{b,f}} - T_{\mathrm{w}}}{T_{\mathrm{bm}} - T_{\mathrm{w}}}, \quad \theta_y^{\mathrm{s}} = \frac{\langle T\rangle_y^{\mathrm{s}} - T_{\mathrm{w}}}{T_{\mathrm{bm}} - T_{\mathrm{w}}} \tag{36}$$
$$Da_{\mathrm{low}} = \frac{K_{\mathrm{low}}}{\varepsilon(w_{\mathrm{c}}+w_{\mathrm{w}})^2}, \quad T_{\mathrm{bm}} = \int_0^{w_{\mathrm{c}}}\langle T\rangle_y^{\mathrm{b,f}}\,\mathrm{d}z,$$
$$\frac{1}{\varepsilon}\int_0^{\varepsilon} U_y\,\mathrm{d}Z = 1, \quad \frac{1}{\varepsilon}\int_0^{\varepsilon}\theta_y^{\mathrm{b,f}}\,\mathrm{d}Z = 1 \tag{37}$$

It is noted that the temperature gradients within the fins are neglected in Eq. (34) since generally the fin efficiency is almost 1 when the aspect ratio is low ($\alpha_{\mathrm{s}} < 1$). For low-aspect-ratio microchannels, permeability K_{low} and interstitial heat transfer coefficient based on one-dimensional bulk mean temperature h_{low} are defined as the following equations:

$$K_{\mathrm{low}} = -\varepsilon H\langle u\rangle_y^{\mathrm{f}} \cdot \left(\left.\frac{\partial u}{\partial y}\right|_{y=H} - \left.\frac{\partial u}{\partial y}\right|_{y=0}\right)^{-1} \tag{38}$$

$$h_{\mathrm{low}} = -\frac{k_{\mathrm{f}}}{T_{\mathrm{w}} - \langle T\rangle_y^{\mathrm{b,f}}}\left(\left.\frac{\partial T}{\partial y}\right|_{y=0}\right) \tag{39}$$

We obtain values of K_{low} and h_{low} from those of the Poiseuille flow between two infinite parallel plates, one of which is subjected to constant temperature and the other to insulated condition [21].

$$K_{\mathrm{low}} = \frac{\varepsilon H^2}{12} \tag{40}$$

$$h_{\mathrm{low}} = (4.861)\frac{k_{\mathrm{f}}}{2H} \tag{41}$$

Once the permeability and the interstitial heat transfer coefficient are determined, velocity and temperature distributions can be obtained by solving Eqs. (32) and (33). The general solution for the dimensionless velocity is given as

$$U_y^{\mathrm{f}} = -P_{\mathrm{low}}\left(1 - \frac{\cosh\left(\frac{1}{\sqrt{Da_{\mathrm{low}}}}\left(\frac{\varepsilon}{2} - Z\right)\right)}{\cosh\left(\frac{\varepsilon}{2\sqrt{Da_{\mathrm{low}}}}\right)}\right) \tag{42}$$

where

$$P_{\mathrm{low}} = -\left(1 - \frac{2\sqrt{Da_{\mathrm{low}}}}{\varepsilon}\tanh\left(\frac{\varepsilon}{2\sqrt{Da_{\mathrm{low}}}}\right)\right)^{-1} \tag{43}$$

The dimensionless temperature for the fluid phase $\theta_y^{\mathrm{b,f}}$ and the dimensionless eigenvalue λ can be obtained by solving Eq. (33) iteratively.

2.3. Asymptotic solutions

2.3.1. Asymptotic solutions for high-aspect-ratio microchannel heat sinks

When the channel height is much larger than the channel width and the solid conductivity is much higher than the fluid conductivity, the governing equations given by Eqs. (19) and (20) can be simplified and analytic solutions for the dimensionless velocity and temperature can be obtained in explicit form. The following relations are assumed:

$$H \gg w_{\mathrm{c}}, \quad k_{\mathrm{s}} \gg k_{\mathrm{f}} \tag{44}$$

Estimating the order of magnitude of each term appearing on the right-hand side of Eq. (19), we have

$$\frac{w_{\mathrm{c}}^2}{H^2} \ll 1 \tag{45}$$

Combining Eqs. (20) and (21) yields

$$\begin{aligned} &-\varepsilon\rho_{\mathrm{f}}c_{\mathrm{f}}u_{\mathrm{m}}U_z^{\mathrm{f}}\frac{\lambda}{2w_{\mathrm{c}}Pe}\theta_z^{\mathrm{b,f}} \\ &\quad= \frac{1}{H^2}\frac{\partial}{\partial Y}\left(k_{\mathrm{fe,high}}\frac{\partial}{\partial Y}\left(\theta_z^{\mathrm{s}} - \frac{1}{h_{\mathrm{high}}a_{\mathrm{high}}H^2}\frac{\partial}{\partial Y}\left(k_{\mathrm{se,high}}\frac{\partial\theta_z^{\mathrm{s}}}{\partial Y}\right)\right)\right) \\ &\qquad+ \frac{1}{H^2}\frac{\partial}{\partial Y}\left(k_{\mathrm{se,high}}\frac{\partial\theta_z^{\mathrm{s}}}{\partial Y}\right) \end{aligned} \tag{46}$$

Estimating the order of magnitude of each term appearing on the right-hand side of Eq. (46), it follows that

$$\left(\frac{k_{\mathrm{f}}}{H^2}, \frac{k_{\mathrm{s}}w_{\mathrm{c}}^2}{H^4}\right) \ll \frac{k_{\mathrm{s}}}{H^2} \tag{47}$$

By using relations presented in Eqs. (45) and (47), the governing equations given by Eqs. (19) and (20) are simplified as

$$P_{\mathrm{high}} = -U_z \tag{48}$$

$$-\varepsilon\rho_{\mathrm{f}}c_{\mathrm{f}}u_{\mathrm{m}}U_z\frac{\lambda}{2w_{\mathrm{c}}Pe}\theta_z^{\mathrm{b,f}} = h_{\mathrm{high}}a_{\mathrm{high}}(\theta_z^{\mathrm{s}} - \theta_z^{\mathrm{b,f}}) \tag{49}$$

Asymptotic solutions for velocity and temperature distributions can be obtained by solving Eqs. (48), (49) and (21). The asymptotic solutions are as follows:

$$U_z = 1 \tag{50}$$

$$\theta_z^{\mathrm{s}} = \frac{\pi}{2}\left(1 + \frac{k_{\mathrm{se,high}}}{H^2h_{\mathrm{high}}a_{\mathrm{high}}}\left(\frac{\pi}{2}\right)^2\right)^{-1}\sin\left(\frac{\pi}{2}Y\right) \tag{51}$$

$$\theta_z^{\mathrm{b,f}} = \frac{\pi}{2}\sin\left(\frac{\pi}{2}Y\right) \tag{52}$$

where

$$P_{\mathrm{high}} = -1 \tag{53}$$

$$\lambda = \frac{4w_{\mathrm{c}}^2}{\varepsilon k_{\mathrm{f}}}\left(\left(\frac{\pi}{2}\right)^{-2}\frac{H^2}{k_{\mathrm{se,high}}} + \frac{1}{h_{\mathrm{high}}a_{\mathrm{high}}}\right)^{-1} \tag{54}$$

2.3.2. Asymptotic solutions for low-aspect-ratio microchannel heat sinks

When the channel height is much smaller than the channel width, the governing equation given by Eq. (32) can be simplified and analytic solutions for the dimensionless velocity and temperature can be obtained without the iterative procedure. When the aspect ratio is very low ($H \ll w_{\mathrm{c}}$), by estimating the order of magnitude of each term appearing on the right-hand side of Eq. (32), we have

$$\frac{\mu_{\mathrm{f}}}{w_{\mathrm{c}}^2} \ll \frac{\mu_{\mathrm{f}}}{H^2} \tag{55}$$

By using this relation, the governing equations given by Eq. (32) are simplified as

$$P_{\mathrm{low}} = -U_y^{\mathrm{f}} \tag{56}$$

Asymptotic solutions for velocity and temperature distributions can be obtained by solving Eqs. (33) and (56). The asymptotic solutions are as follows:

$$U_y^{\mathrm{f}} = 1 \tag{57}$$

$$\theta_y^{\mathrm{b,f}} = \frac{\pi}{2}\cos\left(\frac{\pi}{\varepsilon}\left(Z - \frac{\varepsilon}{2}\right)\right) \tag{58}$$

$$\theta_y^{\mathrm{s}} = 0 \tag{59}$$

where

$$P_{\mathrm{low}} = -1 \tag{60}$$

$$\lambda = \frac{2w_{\mathrm{c}}Pe}{\rho_{\mathrm{f}}c_{\mathrm{f}}u_{\mathrm{m}}}\left(\left(\frac{\pi}{\varepsilon}\right)^2\frac{k_{\mathrm{fe,low}}}{(w_{\mathrm{c}} + w_{\mathrm{w}})^2} + h_{\mathrm{low}}a_{\mathrm{low}}\right) \tag{61}$$

3. Results and discussion

3.1. Velocity and temperature distributions

In order to validate the solutions presented in previous sections, velocity and temperature distributions obtained from general solutions and asymptotic solutions are compared with results of the two-dimensional direct numerical simulation. Two-dimensional numerical solutions are regarded as exact solutions and obtained by solving Eqs. (1) and (2) using the control–volume-based finite difference method. The solutions for high-aspect-ratio heat sinks are compared with numerical results in Figs. 2 and 3. In Fig. 2,

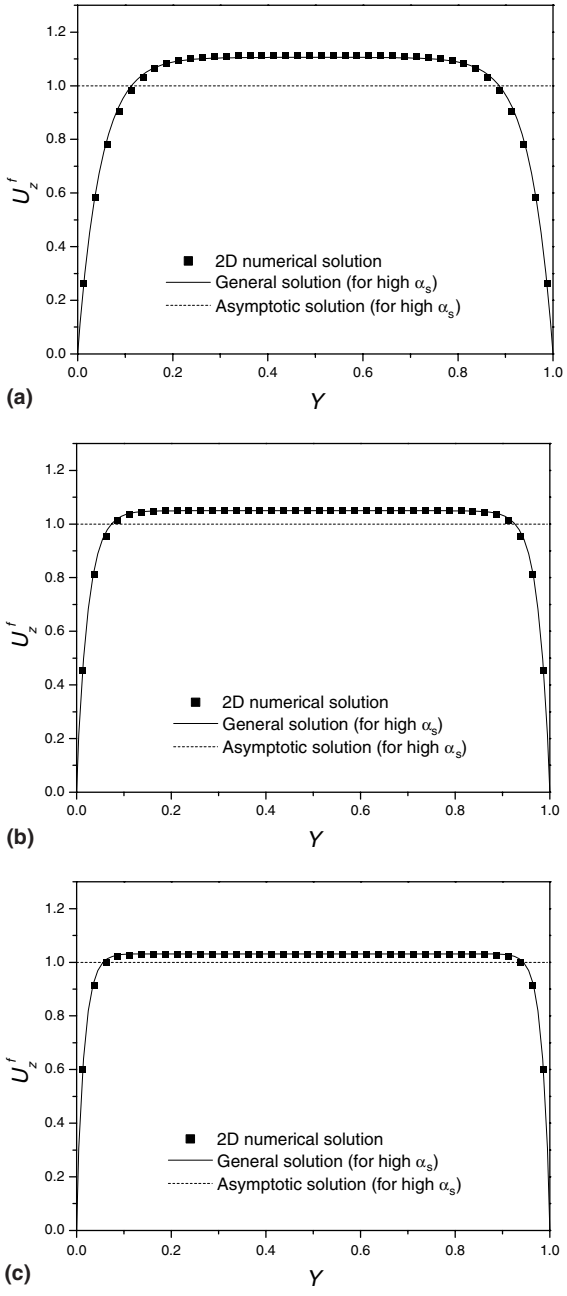

Fig. 2. Dimensionless velocity distributions for high-aspect-ratio heat sinks: (a) $\alpha_s = 6$, (b) $\alpha_s = 12$ and (c) $\alpha_s = 18$.

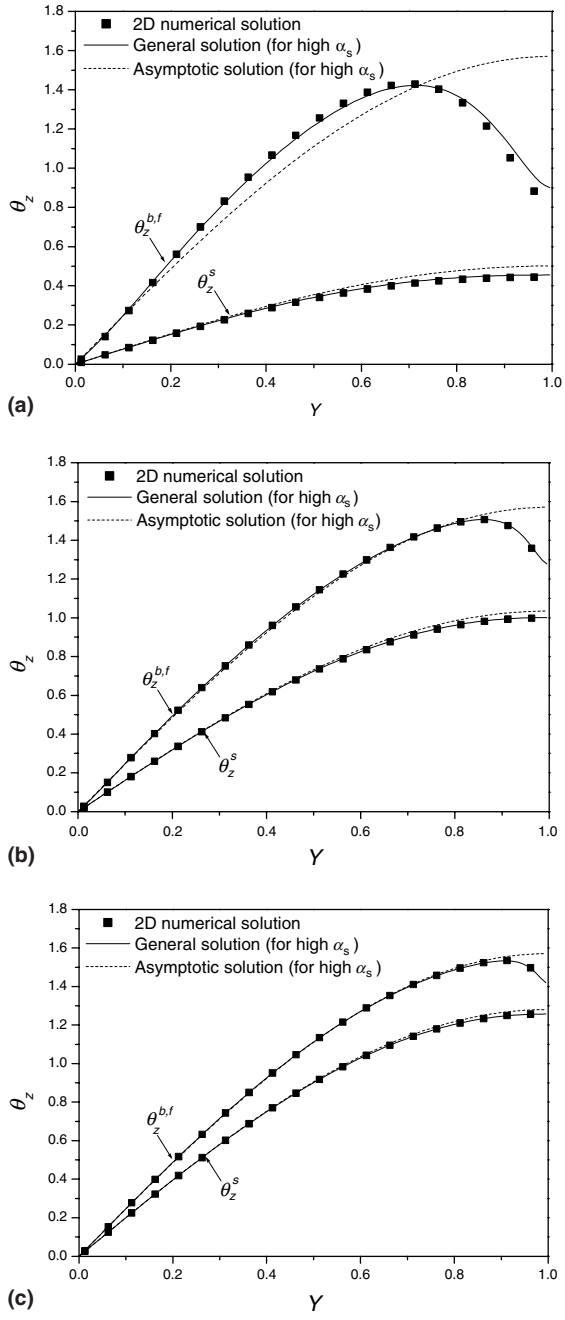

Fig. 3. Dimensionless temperature distributions for high-aspect-ratio heat sinks: (a) $\alpha_s = 6$ ($\varepsilon = 0.5$, $k_f/k_s = 0.00414$), (b) $\alpha_s = 12$ ($\varepsilon = 0.5$, $k_f/k_s = 0.00414$) and (c) $\alpha_s = 18$ ($\varepsilon = 0.5$, $k_f/k_s = 0.00414$).

velocity distributions based on the averaging method are compared with numerical solutions. The general solution accurately reproduces the numerical solution when $\alpha_s > 1$. On the other hand, the asymptotic solution predicts the numerical solution within 5% when $\alpha_s > 10$. Flow is almost uniform (slug flow) throughout microchannels, because viscous shear stress by the fins is dominant. But, there is the variation of the velocity near the boundary, which is due to shear stress by the top and bottom surfaces. In Fig. 3, temperature distributions are presented. The general solutions agree closely with numerical results when $\alpha_s > 1$,

while the asymptotic solutions predict the numerical solutions accurately when $\alpha_s > 10$. As the aspect ratio of microchannel increases, the temperature difference between the fluid phase and the solid phase decreases. This is because heat transfer area between the fins and the fluid increases as the height of a microchannel heat sink becomes larger. In addition, the temperature variation in the solid phase along the fin direction increases as α_s increases. It is due to the fact that the fin efficiency decreases as the height of a microchannel heat sink becomes larger. The solutions for low-aspect-ratio heat sinks are also compared with numerical results in Figs. 4 and 5. As shown in these

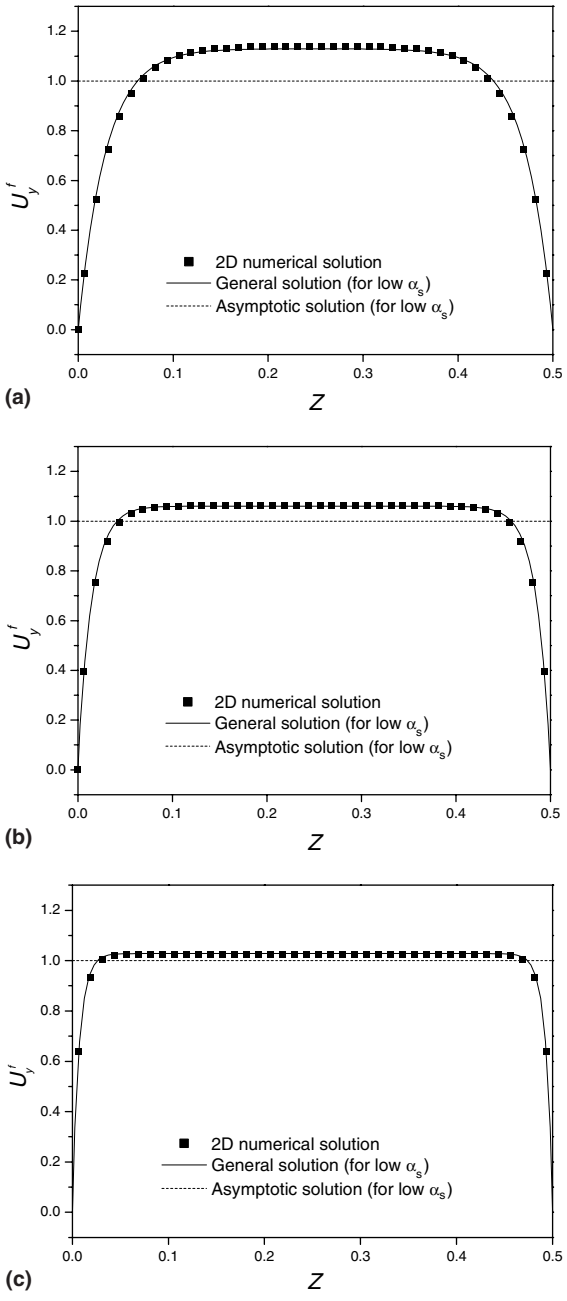

Fig. 4. Dimensionless velocity distributions for low-aspect-ratio heat sinks: (a) $\alpha_s = 0.2$ ($\varepsilon = 0.5$), (b) $\alpha_s = 0.1$ ($\varepsilon = 0.5$) and (c) $\alpha_s = 0.05$ ($\varepsilon = 0.5$).

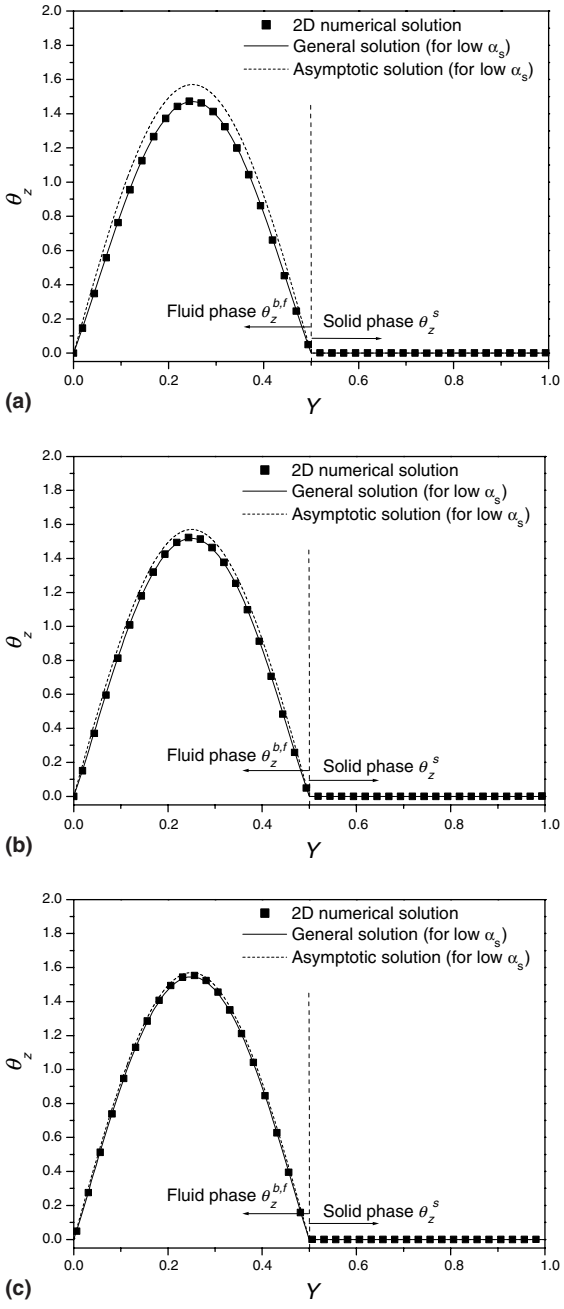

Fig. 5. Dimensionless temperature distributions for low-aspect-ratio heat sinks: (a) $\alpha_s = 0.2$ ($\varepsilon = 0.5$, $k_f/k_s = 0.00414$), (b) $\alpha_s = 0.1$ ($\varepsilon = 0.5$, $k_f/k_s = 0.00414$) and (c) $\alpha_s = 0.05$ ($\varepsilon = 0.5$, $k_f/k_s = 0.00414$).

figures, the general solutions agree closely with numerical results when $\alpha_s < 1$. The asymptotic solutions well predict the numerical solutions when $\alpha_s < 0.1$.

3.2. Friction factor and Nusselt number

In the present paper, the concepts of friction factor and Nusselt number are used for describing macroscopic quantities such as average pressure drop across a channel and average heat transfer rate from a wall. The friction factor is defined as

$$f = \frac{\tau_w}{\frac{1}{2}\rho u_m^2} \tag{62}$$

According to Eq. (53), the friction factor in the high-aspect-ratio limit ($\alpha_s \to \infty$) is expressed as

$$fRe_{D_h} = 24\left(\frac{\alpha_s}{\alpha_s + 1}\right)^2 \tag{63}$$

where D_h is the hydraulic diameter of the channel. From Eq. (60), the friction factor in the low-aspect-ratio limit ($\alpha_s \to 0$) is given as

$$fRe_{D_h} = 24\left(\frac{1}{\alpha_s + 1}\right)^2 \tag{64}$$

The friction factors for high-aspect-ratio microchannel heat sinks are shown in Fig. 6. When $1 < \alpha_s < 20$, the friction factor increases as the aspect ratio increases. For large aspect ratio ($\alpha_s > 20$), the behavior of the friction factor approaches that of the flow between two infinite parallel plates. The friction factors for low-aspect-ratio microchannel heat sinks are shown in Fig. 7. As we can see, the friction factor increases as the aspect ratio decreases when $0.05 < \alpha_s < 1$. For small aspect ratio ($\alpha_s < 0.05$), the behavior of the friction factor also approaches that of the flow between two infinite parallel plates.

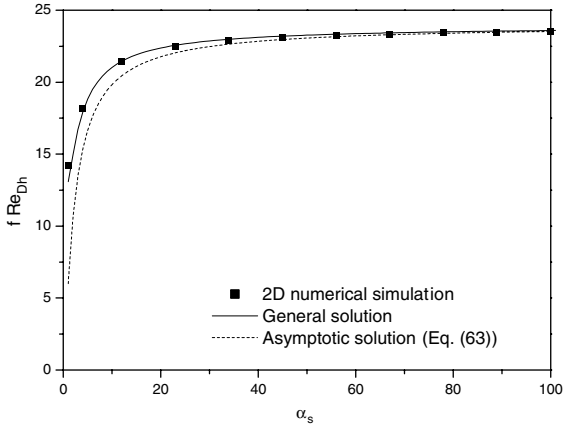

Fig. 6. Friction factors for high-aspect-ratio heat sinks.

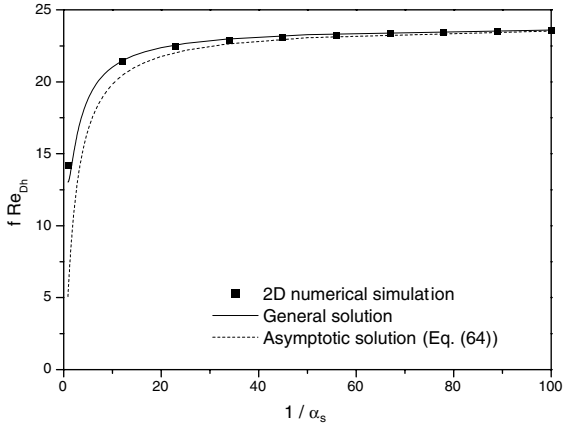

Fig. 7. Friction factors for low-aspect-ratio heat sinks.

The Nusselt number is given as

$$Nu_H = \frac{q''}{(T_w - T_{bm})}\frac{H}{k_f} = \frac{\alpha_s^2 \varepsilon}{4}\lambda \tag{65}$$

According to Eqs. (27) and (54), the Nusselt number for $\alpha_s \to \infty$ is given as

$$Nu_H = \frac{\alpha_s^2 \varepsilon}{4}\left(\frac{3.341D + 1.092 - \sqrt{(3.341D + 1.092)^2 - 1.229D}}{0.01864D}\right) \tag{66}$$

where $D = \frac{k_f}{k_s}\frac{\varepsilon}{1-\varepsilon}\alpha_s^2$. From Eq. (61), the Nusselt number for $\alpha_s \to 0$ is given as

$$Nu_H = \frac{\alpha_s^2 \varepsilon}{4}\left(4\pi^2 + \frac{9.722}{\alpha_s^2}\right) \tag{67}$$

Eq. (66) shows that the Nusselt number depends on the conductivity ratio, the aspect ratio, and the porosity. The effect of these parameters on the Nusselt number is illustrated in Figs. 8 and 9. The Nusselt numbers for high-aspect-ratio microchannel heat sinks are shown in Fig. 8. When $\alpha_s > 1$, the Nusselt number increases as the aspect ratio of the microchannel increases, because the heat transfer area of the fins increases. The Nusselt number increases as the porosity decreases. This is based on the fact that the heat transfer along the fins increases as the fin thickness increases. The Nusselt number increases as the conductivity ratio increases. This is because the fin efficiency increases as the solid conductivity becomes larger. On the other hand, the Nusselt numbers for low-aspect-ratio microchannel heat sinks are shown in Fig. 9. As we can see, the Nusselt number increases as the porosity of the microchannel increases, because the heat transfer area of the bottom wall increases. The Nusselt number does not strongly depend on the conductivity ratio because the fin efficiency for the low-aspect-ratio heat sink is almost 1 and does not vary considerably.

3.3. Thermal resistance of the microchannel heat sink

The thermal performance of the microchannel heat sink can be evaluated by the concept of thermal resistance. Generally, the thermal resistance is defined as the temperature difference between the heat sink base temperature at the outlet and the fluid bulk mean temperature at the inlet per unit heat flow rate.

$$R_\theta = \frac{T_{w,out} - T_{bm,in}}{q} \tag{68}$$

For the constant temperature boundary condition, the thermal resistance is given as

$$R_\theta = \frac{1}{\rho_f c_f \dot{Q}\left(1 - \exp\left(-\frac{2}{\alpha_s^2 \varepsilon}\frac{Nu_\mu}{Pe}\frac{L}{w_c}\right)\right)} \tag{69}$$

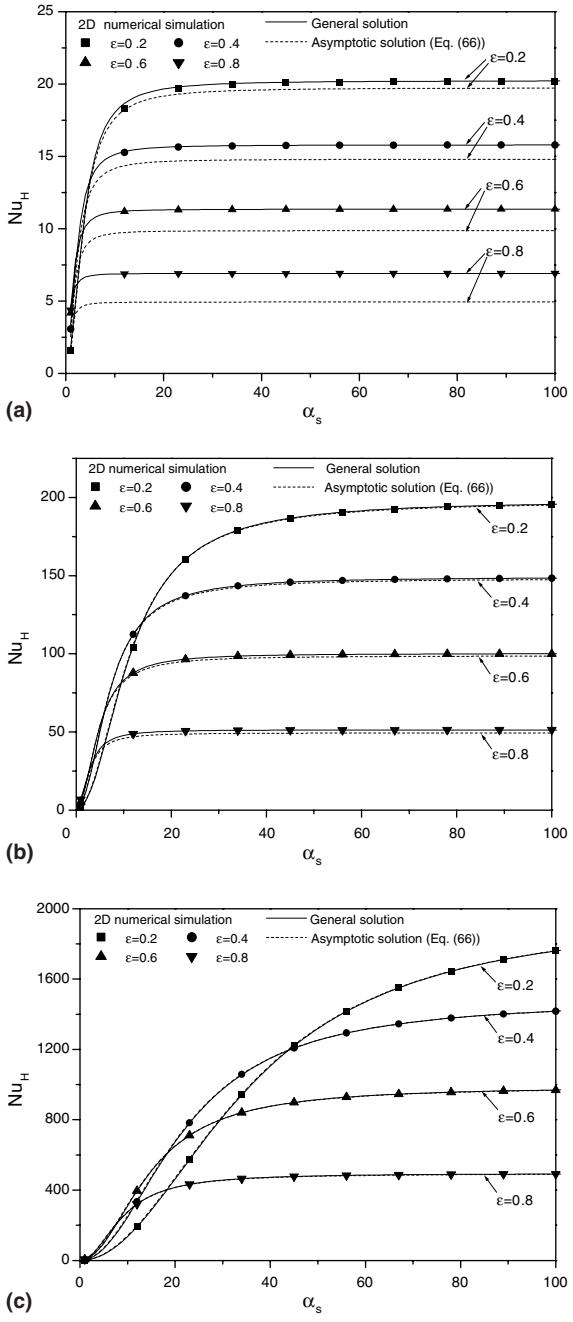

Fig. 8. Nusselt numbers for high-aspect-ratio heat sinks: (a) $k_s/k_f = 10$, (b) $k_s/k_f = 100$ and (c) $k_s/k_f = 1000$.

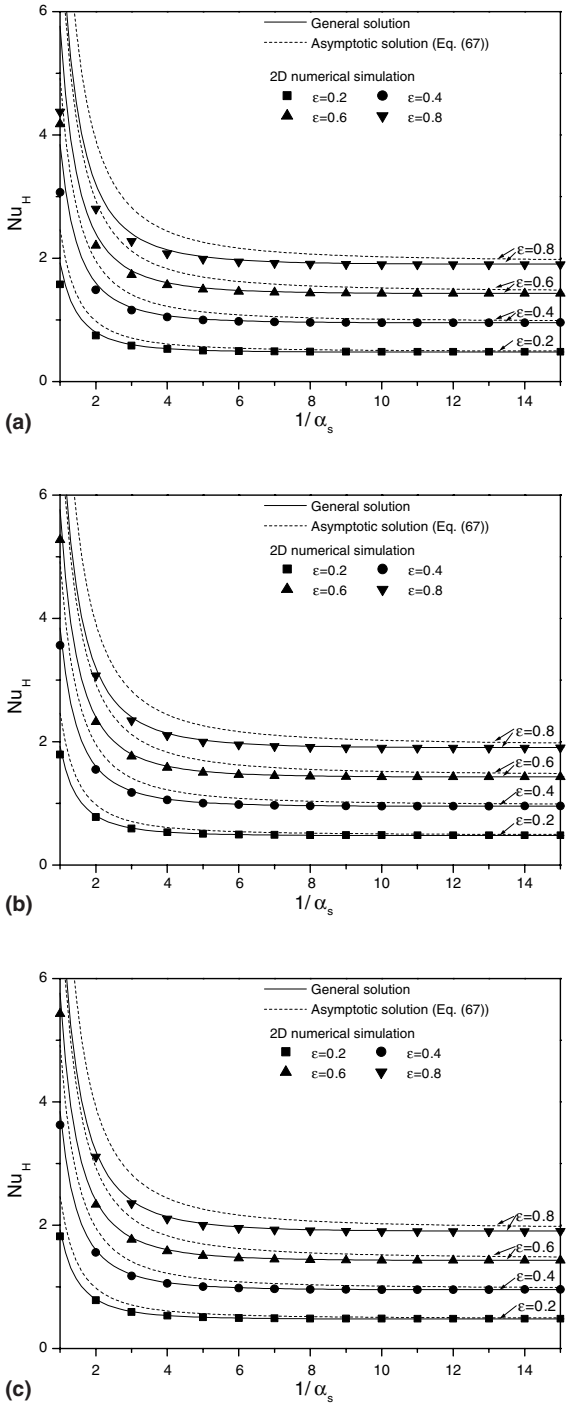

Fig. 9. Nusselt numbers for low-aspect-ratio heat sinks: (a) $k_s/k_f = 10$, (b) $k_s/k_f = 100$ and (c) $k_s/k_f = 1000$.

where $\dot{Q}$ is the flow rate, When the pumping power C_{pump} is fixed, the flow rate is given as

$$\dot{Q} = \sqrt{\frac{\varepsilon}{2\mu}\frac{C_{\text{pump}}}{fRe}\frac{D_h^2 WH}{L}} \tag{70}$$

Figs. 10 and 11 depict the thermal resistances for various heights. The thermal resistances calculate using the asymptotic solution, the general solution, and the numerical simulation, respectively. Results of the two-dimensional numerical simulation can be regarded as exact values for the thermal resistance. As shown in Figs. 10 and 11, results from the general solution match well with numerical results. In addition, asymptotic solution is simple, but accurately predicts thermal resistance. As we can see, the total resistance has a minimum value. This is because the flow rate and the heat transfer area increase but the fin efficiency decreases as the height of the microchannel heat sink becomes larger. Fig. 12 presents the thermal resistances for

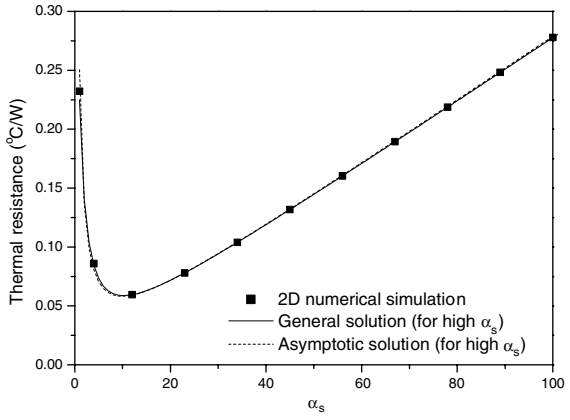

Fig. 10. Thermal resistances for high-aspect-ratio heat sinks ($w_c = w_w = 50\ \mu m$, $L = W = 1$ cm, $k_s = 148$ W/mK, $k_f = 0.613$ W/mK, $C_{pump} = 2.56$ W).

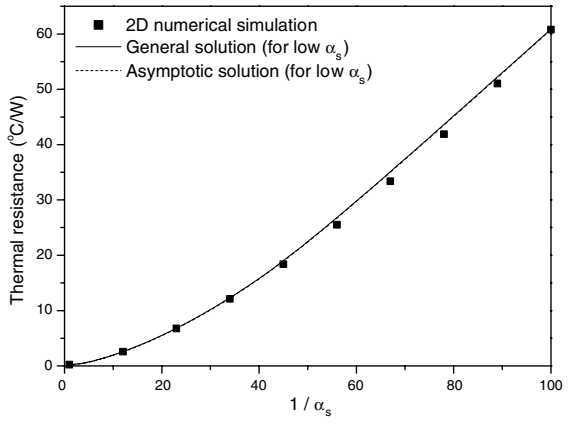

Fig. 11. Thermal resistances for low-aspect-ratio heat sinks ($w_c = w_w = 50\ \mu m$, $L = W = 1$ cm, $k_s = 148$ W/mK, $k_f = 0.613$ W/mK, $C_{pump} = 2.56$ W).

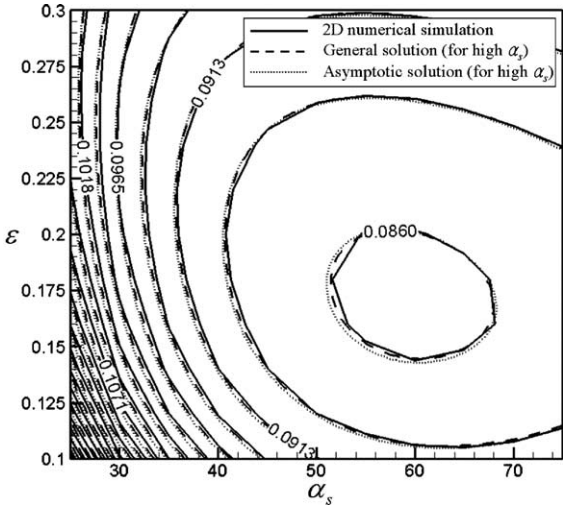

Fig. 12. Thermal resistances (°C/W) for various aspect ratios and porosities ($H = 2$ mm, $L = W = 1$ cm, $k_s = 148$ W/mK, $k_f = 0.613$ W/mK, $C_{pump} = 2.56$ W).

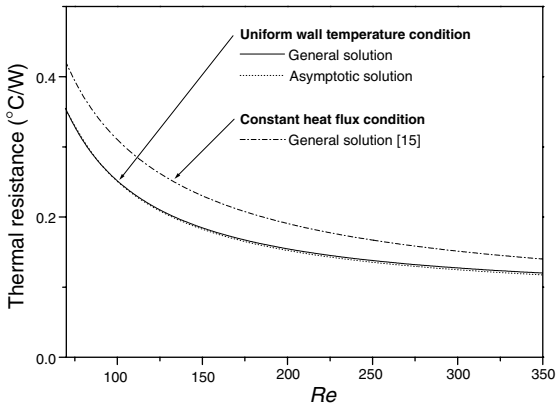

Fig. 13. Comparison between thermal resistances for uniform wall temperature and thermal resistances for constant heat rate.

various aspect ratios and porosities. As illustrated in Fig. 12, there exists a set of the aspect ratio and the porosity for which the thermal resistance is minimized. This is because the flow rate increases but the fin efficiency decreases as the porosity becomes larger, and because the heat transfer area increases but the flow rate and the fin efficiency decrease as the aspect ratio becomes larger. It is worth mentioning that the optimum values obtained by

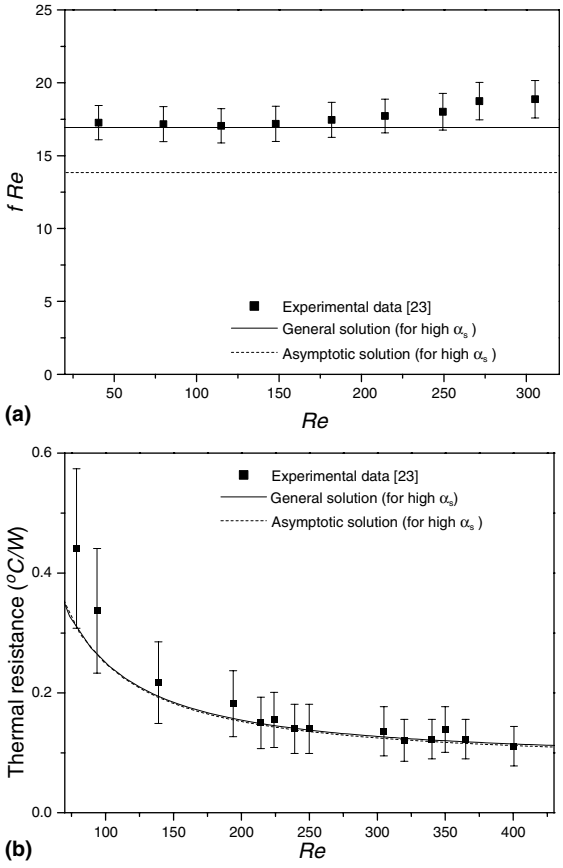

Fig. 14. Comparison between results from the models and experimental data for (a) friction factors and (b) thermal resistances.

using averaging approach are in close agreement with numerical results. These dimensions are important to design a microstructure for microchannel heat sinks. In addition, Fig. 13 shows the comparison between thermal resistances for the uniform wall temperature and constant heat rate conditions. As we can see, the thermal resistance for the uniform wall temperature is about 10% less than that for constant heat rate condition.

3.4. Comparison of solutions with experimental data

In addition to the comparison with the numerical results, the present results are also compared with experimental data by Kawano et al. [23]. Fig. 14 presents the friction factors and the thermal resistances. As shown in Fig. 14, results from the general solution lie within the range of experimental uncertainties. The friction factors obtained from the asymptotic solution underpredict the experimental data. It is due to the facts that Kawano et al. performed experiment in which aspect ratio of microchannel is 3.16 and that the asymptotic solution deviates from exact value when $\alpha_s < 10$.

4. Conclusion

In the present paper, we conduct a thermal analysis of microchannel heat sinks subject to the uniform wall temperature condition by using the modeling method based on an averaging approach. The solutions for the velocity and temperature distributions are obtained by solving one-dimensional averaged governing equations without resorting to a two-dimensional direct numerical simulation. General solutions for both high-aspect-ratio and low-aspect-ratio microchannel heat sinks are presented. Asymptotic solutions in high-aspect-ratio and low-aspect-ratio limits are given in explicit form. The solutions proposed in the paper are validated by comparing them with the results of direct numerical simulation. The general solution exactly reproduces the numerical solution and the asymptotic solution predicts the numerical solution within 5% when $\alpha_s < 0.1$ or $\alpha_s > 10$. The friction factors and the Nusselt numbers for microchannel heat sinks are obtained from the presented solutions. As the aspect ratio increases, the friction factor decreases when $0.05 < \alpha_s < 1$ and then increases when $1 < \alpha_s < 20$. The friction factor does not vary considerably when $\alpha_s < 0.05$ or $\alpha_s > 20$. It is shown that the Nusselt number depends on the conductivity ratio, the aspect ratio, and the porosity. Finally, characteristics of the thermal resistance of the microchannel heat sink are discussed. There exists a set of the aspect ratio and the porosity for which the thermal resistance is minimized. This is because the flow rate increases but the fin efficiency decreases as the porosity becomes larger, and because the heat transfer area increases but the flow rate and the fin efficiency decrease as the aspect ratio becomes larger. Generally, the thermal resistance for the uniform wall temperature condition is about 10% less than that for the constant heat rate condition.

References

[1] S. Oktay, R.J. Hannemann, A. Bar-Cohen, High heat from a small package, Mech. Eng. 108 (3) (1986) 36–42.
[2] A. Bar-Cohen, Thermal management of electric components with dielectric liquids, in: J.R. Lloyd, Y. Kurosaki (Eds.), Proceedings of ASME/JSME Thermal Engineering Joint Conference vol. 2 (1996) 15–39.
[3] F.P. Incropera, Convection heat transfer in electronic equipment cooling, J. Heat Transfer 110 (1988) 1097–1111.
[4] W. Nakayama, Thermal management of electronic equipment: a review of technology and research topics, Appl. Mech. Rev. 39 (12) (1986) 1847–1868.
[5] D.B. Tuckerman, R.F.W. Pease, High-performance heat sinking for VLSI, IEEE Electron Dev. Lett. 2 (1981) 126–129.
[6] R.J. Phillips, Microchannel heat sinks, in: A. Bar-Cohen, A.D. Kraus (Eds.), Advances in Thermal Modeling of Electronic Components and Systems, vol. 2, ASME Press, New York, 1990, pp. 109–184.
[7] J.S. Goodling, R.W. Knight, Optimal design of microchannel heat sink: a review, Optimal Des. Therm. Syst. Components 279 (1994) 65–77.
[8] R.W. Knight, J.S. Goodling, D.J. Hall, Optimal thermal design of forced convection heat sinks—analytical, J. Electron. Packag. 113 (1991) 313–321.
[9] R.W. Knight, D.J. Hall, J.S. Goodling, R.C. Jaeger, Heat sink optimization with application to microchannels, IEEE Trans. Components Hybrids Manuf. Technol. 15 (1992) 832–842.
[10] G.N. Ellison, Thermal Computations for Electronic Equipment, Robert E. Krieger Publishing Company, Malabar, 1989, pp. 118–120.
[11] S.J. Kim, Methods for thermal optimization of microchannel heat sinks, Heat Transfer Engineering 25 (1) (2004) 37–49.
[12] C.Y. Zhao, T.J. Lu, Analysis of microchannel heat sinks for electronics cooling, Int. J. Heat Mass Transfer 45 (2002) 4857–4869.
[13] J.C.Y. Koh, R. Colony, Heat transfer of microstructures for integrated circuits, Int. Comm. Heat Mass Transfer 13 (1986) 89–98.
[14] C.L. Tien, S.M. Kuo, Analysis of forced convection in microstructures for electronic system cooling, in: Proceedings of the International Symposium on Cooling Technology for Electronic Equipment, 1987, pp. 217–226.
[15] S.J. Kim, D. Kim, Forced convection in microstructures for electronic equipment cooling, J. Heat Transfer 121 (1999) 639–645.
[16] S.J. Kim, D. Kim, D.Y. Lee, On the local thermal equilibrium in microchannel heat sinks, Int. J. Heat Mass Transfer 43 (2000) 1735–1748.
[17] S.J. Kim, J.M. Hyun, Porous-medium approach for thermal analysis of heat transfer devices, in: D.B. Ingham, I. Pop (Eds.), Transport Phenomena in Porous Media, fifth ed., Pergamon Press (in press).
[18] T.P. Cotter, Principles and prospects for micro heat pipe, in: J.R. Lloyd, Y. Kurosaki (Eds.), Proceedings of Fifth International Heat Pipe Conference, Tsukuba, Japan, 1984, pp. 328–335.
[19] F.P. Incropera, D.P. DeWitt, Fundamentals of Heat and Mass Transfer, fifth ed., John Wiley & Sons, Inc., New York, 2002, pp. 473–475.
[20] V.C. Slattery, Advanced Transport Phenomena, Cambridge University Press, Cambridge, 1999, pp. 194–197.
[21] R.K. Shah, A.L. London, Laminar Flow Forced Convection in Ducts, Academic Press, London, 1978, pp. 194–197.
[22] A. Bejan, Convective Heat Transfer, second ed., John Wiley & Sons, Inc., New York, 1995, pp. 115–118.
[23] K. Kawano, K. Minakami, H. Iwasaki, M. Ishizuka, Micro channel heat exchanger for cooling electrical equipment, in: Application of Heat Transfer in Equipment, Systems and Education, ASME HTD-351-3/PID-3, 1998, pp. 173–180.